Diversity and metabolism of xylose and glucose fermenting microbial communities in sequencing batch or continuous culturing

Rombouts, Julius L.; Mos, Galvin; Weissbrodt, David G.; Kleerebezem, Robbert; Van Loosdrecht, Mark C.M.

DOI
10.1093/femsec/fiy233

Publication date
2019

Document Version
Accepted author manuscript

Published in
FEMS Microbiology Ecology

Diversity and metabolism of xylose and glucose fermenting microbial communities in sequencing batch or continuous culturing

Julius L. Rombouts*, Galvin Mos, David G. Weissbrodt[§] and Robbert Kleerebezem[§], Mark C.M. Van Loosdrecht[§]

Delft University of technology, Department of Biotechnology, Van der Maasweg 9, 2629 HZ Delft, the Netherlands.

* Corresponding author, julesrombouts@gmail.com, +316 15654428

[§] Shared senior authorship

Submission to FEMS Microbiology Ecology

Abstract

A mechanistic understanding of microbial community establishment and product formation in open fermentative systems can aid the development of bioprocesses utilising organic waste. Kinetically, a single rate-limiting substrate is expected to result in one dominant species. Four enrichment cultures were operated to ferment either xylose or glucose in a sequencing batch reactor (SBR) or a continuous-flow

stirred tank reactor (CSTR) mode. The combination of 16S rRNA gene-based analysis and fluorescence *in situ* hybridization revealed no complete dominance of one species in the community. The glucose-fed and xylose-fed SBR enrichments were dominated >80% by one species. *Enterobacteriaceae* dominated the SBRs enrichments, with *Citrobacter freundii* dominant for xylose *and Enterobacter cloacae* for glucose. *Clostridium*, *Enterobacteriaceae* and *Lachnospiraceae* affiliates dominated the CSTRs enrichments. Independent of substrate, SBR communities displayed 2-3 times higher biomass specific rate of substrate uptake (q_s^{max}) and 50% lower biomass yield on ATP, to CSTR communities. Butyrate production was linked to dominance of *Clostridium* and low q_s^{max} (1.06 $Cmol_s$ $Cmol_x^{-1}$ h^{-1}), while acetate and ethanol production was linked to dominance of *Enterobacteriaceae* and *Lachnospiraceae* and high q_s^{max} (1.72 $Cmol_s$ $Cmol_x^{-1}$ h^{-1} and higher). Overall, more diversity than expected through competition was observed, indicating mutualistic mechanisms might shape microbial diversity.

Keywords: Mixed culture fermentation – Bioreactor operation – Microbial diversity– r/K selection – Product spectrum – Kinetics

Introduction

The global aim of most societies to develop more circular economies (Ghisellini, Cialani and Ulgiati 2016) urges for a better use of organic waste as a resource. Until now, anaerobic digestion is the most common technology used to valorise this waste in the form of biogas. Several novel bio-based options that provide extra value to resource recovery are arising such as the production of polyhydroxyalkanoates

(Kleerebezem and van Loosdrecht 2007), alginate-like exopolymers (Lin *et al.* 2010), or medium chain length fatty acids (Spirito *et al.* 2014). The first step in these production routes consists of the conversion of polymeric carbohydrates into volatile fatty acids (VFAs) in a mixed-culture fermentative process (Marshall, LaBelle and May 2013). The alignment of VFA production to subsequent processing requires the identification of factors that drive product formation in microbial communities as function of process conditions. First attempts to describe steady-state patterns of mixed culture fermentation as function of an environmental parameter have provided incomplete insights in the product formation pathways established (Rodriguez *et al.* 2006; González-Cabaleiro, Lema and Rodríguez 2015). Observed product spectra at neutral pH could not be simulated properly using these models oriented to ATP production maximisation, indicating incomplete model assumptions. To aid model-based developments there is a need for experimental studies giving a more comprehensive insight into fermentation of specific carbohydrates into VFAs.

Xylose and glucose are the most abundant monomers found in lignocellulosic biomass (Anwar, Gulfraz and Irshad 2014). Fermentation of glucose or xylose can lead to different products, such as lactic acid, ethanol, hydrogen, and VFAs (Figure 1). Xylose can be fermented through the pentose phosphate pathway (PPP) or the phosphoketolase pathway (PKP), resulting in a different stoichiometry. Using the PKP, 40% of the carbon is directly converted to acetate, while the remaining carbon enters into glycolysis. In PPP, all carbon is converted to intermediates for glycolysis, thereby bringing all carbon to pyruvate first (Figure 1). In the first part of glycolysis, one glucose is converted to pyruvate producing four electrons that can be transferred to NADH. If one acetate is produced, a net amount of one NADH is produced. These

electrons cannot be transferred from NADH to hydrogen, as NADH does not possess sufficient energy to drive this reaction (-320 mV and -414 mV for NADH and hydrogen respectively, Buckel and Thauer 2013). Hydrogen is produced through ferredoxin (-400 mV), which is produced when oxidising pyruvate to Acetyl-CoA (Figure 1). The NADH surplus is oxidised by other fermentative pathways, *e.g.* ethanol production, thereby stoichiometrically coupling acetate and ethanol formation. Recently, electron bifurcation has been proposed as a metabolic strategy in *Clostridium pasteurianum* (Buckel and Thauer 2013) used to conserve energy in fermentation by directly coupling acetate and butyrate formation (Li *et al.* 2008). This mechanism has been successfully incorporated in balancing of NADH of product spectra over a range of pH values (Regueira *et al.* 2018).

Microbial enrichment cultures offer a powerful way of studying the establishment of a specific microbial niche (Beijerinck 1901), depending on the ecological conditions applied, such as pH, temperature, redox couple supplied, nutrients among others. Glucose fermentation has been relatively widely studied, including impacts of pH (Fang and Liu 2002; Temudo, Kleerebezem and van Loosdrecht 2007), temperature (Zoetemeyer *et al.* 1982), solid retention time (SRT) (Chunfeng *et al.* 2009), redox potential (Ren *et al.* 2007), inoculum type (Rafrafi *et al.* 2013), or hydrogen partial pressure (de Kok *et al.* 2013). Xylose is much less studied but its fermentation has been compared to glucose fermentation previously (Temudo *et al.* 2009).

Most studies have been conducted in continuous-flow stirred tank reactors (CSTR), under which regime one substrate is continuously limiting (*i.e.*, operation at low residual concentration). In CSTR systems, affinity dictates the selection: organisms

establishing the lowest residual substrate concentration (C_s) will dominate the enrichment (Kuenen 2014). Affinity is governed by both the maximum biomass specific growth rate (μ^{max}) and the affinity constant for substrate (K_s). Organisms competing for a substrate in a CSTR environment can, besides optimising their μ^{max}, optimise their K_s value to actively take up the substrate and dominate the microbial community.

In a sequencing batch reactor (SBR) operation, substrate is supplied in a pulse, leading to a high concentration in the environment of the microorganisms during most of the time that substrate is taken up. Organisms with the highest μ^{max} will eventually dominate when substrate uptake is directly coupled to growth. The batch selective environment is traditionally used in microbiology to enrich and isolate organisms, using the shake-flask approach in combination with dilution series. Consequently, fast-growing microorganisms are overrepresented in databases of pure cultures (Prakash *et al.* 2013).

For both CSTR and SBR environments, μ^{max} is a selective force, which is a function of the biomass specific rate of substrate uptake (q_s^{max}), the biomass yield on substrate ($Y_{x,s}$) and the maintenance rate on substrate (m_S) (Pirt 1965). From a kinetic point of view, the microorganism with the highest competitive advantage in the environment will eventually outcompete the other microorganisms, which is either the highest μ^{max} (in SBR) or highest affinity (in CSTR) on glucose or xylose. Ultimately, we aim to investigate the hypothesis if limiting a single substrate in an enrichment culture leads to the enrichment of a single microbial species. From a competition point of view, one limiting substrate will select for the most competitive

126 microorganism. Given enough generations or SRTs, this microorganism will
127 eventually dominate the enrichment culture.
128
129 Next to microbial competition on substrate, the different pathways for product
130 formation are competing within microorganisms. Anabolism needs chemical energy in
131 the form of ATP to synthesize biomass. Under similar anabolic efficiency, the
132 catabolic pathway that yields more ATP per substrate ($Y_{ATP,s}$) leads to the highest
133 $Y_{x,s}$. Harvested ATP can also be used for active substrate transport. Hereby,
134 microorganisms lower their K_s and thereby create a lower C_s to sustain their selection
135 in a CSTR environment. Fermentative microorganisms are known to choose between
136 a high flux pathway (optimizing q_s^{max}) or a high yield pathway (optimising $Y_{ATP,s}$),
137 which is best described by lactate versus acetate and ethanol formation in
138 *Lactobacillus casei* (De Vries *et al.* 1970). Under CSTR cultivation, at high dilution
139 rates lactate is formed and at low dilution rates acetate, ethanol and formate are
140 formed. Lactate formation yields 2 ATP from 1 glucose, while acetate and ethanol
141 yield 3 ATP from 1 glucose. Thus lactate production is linked to high q_s^{max}, while
142 acetate and ethanol production is linked to high $Y_{ATP,s}$. Thus, a microorganism will
143 preferentially involve a metabolic pathway that maximizes $Y_{ATP,s}$ and/or q_s^{max} in a
144 SBR environment and $Y_{ATP,s}$, q_s^{max} and/or K_s in a CSTR environment.
145 Here, we investigated whether SBR or CSTR environments fermenting either xylose
146 or glucose enrich for an equal microbial community composition and result in
147 equivalent metabolism and kinetics. Three environmental settings were applied to
148 enrich for fermentative microorganisms: (1) a mineral medium with only glucose or
149 xylose as carbon source for fermentation; (2) a combination of temperature, pH, and
150 SRT to select mainly for primary fermentative microorganisms; and (3) suspended

cell cultures. The experimental set up was replicated from Temudo et al. (2009) for a direct comparison of results. The catabolic products, q_s^{max}, and $Y_{x,s}$ were measured for each enrichment in steady state in order to verify if a certain stoichiometry was linked to a certain metabolic strategy. In parallel, we analysed the microbial community compositions to test the microbial diversity hypothesis for enrichment on single substrates, and to link community structures to fermentative products and metabolic strategies.

Materials and methods

Enrichment

All enrichments were performed in 3-L jacketed bioreactors (Applikon, the Netherlands) with working volumes of 2 L. pH was maintained at 8.0 ± 0.1 using NaOH at 4 mol L^{-1} and HCl at 1 mol L^{-1}. Temperature was maintained at 30°C ± 0.1 using a E300 thermostat (Lauda, Germany). The cultures were stirred constantly at 300 rpm. Anaerobic conditions were maintained by sparging the reactor with a flow of 576 mmol N_2 h^{-1} and off-gas was cooled to 5°C using a gas condenser. For the SBRs, a hydraulic retention time (HRT) of 8 h was maintained by removing 1 L of culture per cycle under a cycle time set to 4 h. For CSTRs, the HRT was directly linked to the dilution rate applied.

The synthetic cultivation medium was identical to the one used by Temudo et al. (2007) using 4 g of either xylose or glucose as carbon source per litre. The carbon source and the ammonium, phosphate and trace elements were fed separately from

12.5× concentrated stock solutions and diluted using N_2-sparged demineralized water. Connected to the base pump was a pump supplying 3% (v:v) antifoam C (Sigma Aldrich, Germany), which ensured a flow of 3-5 mL h^{-1} or 14-17 mL $cycle^{-1}$. The glucose and xylose solutions were sterilized at 110°C for 20 min.

The inoculum was obtained from cow rumen through a butcher in Est, the Netherlands, and on the same day, transported to lab at room temperature and filtered on 200 µm and aliquoted in 50-mL portions, and frozen at -20°C using 10% glycerol. The seed biomass was then thawed on ice before adding 10 mL to the reactor to start each enrichment culture. When a full first batch was performed the CSTRs were set to continuous mode and the SBRs were set in cycle mode, gradually moving from 24-h to 12-h and 6-h in 3 days to the final desired 4-h cycles to maintain a HRT of 8 h. Steady state was assumed if during a period of at least 5 days no variation was in the product concentrations.

Analytical methods

Samples from the reactors were immediately filtered on 0.45 µm polyvinylidine fluoride membranes (Millipore, USA) and stored at -20°C until analysis. VFAs (formate to valerate), lactate, succinate, ethanol, glucose and xylose were analysed using high performance liquid chromatograph (HPLC) equipped with an Aminex HPX-87H column (BioRad, USA) maintained at 60 °C and coupled to ultraviolet (UV) and refraction index (RI) detectors (Waters, USA), using phosphoric acid at 0.01 mol L^{-1} as eluent. For high butyrate concentrations above 1 mmol L^{-1}, samples were analysed using gas chromatography (GC), since butyrate overlapped with ethanol on

the RI detector of the HPLC. GC was performed using a Chrompack 9001 (Agilent, USA) equipped with an injector maintained at 180°C, a fused-silica capillary column of 15 m × 0.53 mm HP-INNOWax (Agilent, USA) equilibrated at 80°C for alcohols with helium as carrier gas, and a flame ionization detector set at 200°C. Glycerol was detected using an enzymatic assay relying on glycerokinase, pyruvate kinase and L-lactate dehydrogenase, measuring NADH depletion at 340 nm (Megazyme, Ireland).

The off-gases were monitored on-line for H_2 and CO_2 by a connection to a NGA 2000 MLT 1 Multicomponent analyser (Rosemount, USA). Data acquisition (base, H_2, CO_2) was made using a BBI systems MFCS/win 2.1 (Sartorius, Germany).

Biomass concentration was measured using a standard method which relies on centrifugation to separate the cells from the medium (APHA, 1998). This analysis was coupled to absorbance measurement at 660 nm to establish a correlation. Absorbance values were used to calculate the biomass concentration during the batch experiments.

Cycle analysis

To characterise one cycle in SBR mode, one full cycle was sampled and product and biomass concentrations were measured in parallel to H_2 and CO_2 in the off-gas. In the CSTRs, one litre of volume was removed and one litre of medium was added to finally obtain a concentration of 4 g L^{-1} of either xylose or glucose together with a stoichiometric amount of other nutrients. Sampling and off-gas analysis were carried out as in the SBRs.

Microbial community analysis

Genomic DNA was extracted using the Ultra Clean Soil DNA extraction kit (MOBIO laboratories, USA) following manufacturer's instructions, with the exception of heating the samples for 5 minutes at 65°C prior to bead beating. Highly molecular DNA was obtained (>10 kb) with a concentration of 10 ng μL^{-1} or higher. Extracted DNA was stored at -20°C until further use.

Analysis of 16S rRNA gene-based amplicon sequencing was conducted to get an overview of the predominant populations in the enrichments in time. The extracted DNA was sent for amplification and sequencing at a commercial company (Novogene, China). Amplification was achieved using the universal primer set 341f / 806r targeting the V3-V4 region of the 16S rRNA gene (Table S1). All polymerase chain reactions (PCR) were carried out in 30 µL reactions with 15 µL of Phusion® High_fidelity PCR Master Mix (New England Biolabs, USA), 0.2 µmol L^{-1} of forward and reverse primers and 10 ng template DNA. Thermal cycling started with an initial denaturation at 98°C for 10 s, annealing at 50°C for 30 s and elongation at 72°C for 60 s and ending with 72°C for 5 min. These pools of amplicon sequences were then sequenced using an IlluminaHiSeq2500 platform. The sequencing datasets were cleaned and trimmed according to Jia *et al.* (2016) and processed with Qiime (Caporaso *et al.* 2010) using UCLUST with a 97% stringency to yield operational taxonomic units (OTUs). OTUs were taxonomically classified using the RDP classifier (Wang *et al.* 2007) with 0.85 confidence interval against the Greengenes database release of August 2013 (DeSantis *et al.* 2006). Double check of OTUs identity factors

was then obtained by alignment against the NCBI RefSeq database using the basic alignment search tool for nucleotides (BLASTn) (Johnson *et al.* 2008).

Cloning-sequencing was conducted to obtain species level information. The near-complete 16S rRNA gene was amplified using the primers GM3f and GM4r (Table S1). The PCR products were purified using QIAquick PCR purification kit (QIAGEN, Germany), ligated, and transformed into competent *Escherichia coli* cells using the TOPO TA Cloning Kit (Invitrogen, USA). Transformed cells were plated on Luria-Bertani medium plates containing 50 µg kanamycin mL^{-1}. After overnight incubation at 37°C, clones were randomly selected for amplification of the 16S insert into the PCR4-TOPO vector using the M13f and M13r primers (Table S1). Depending on the diversity of the sample, 8 to 55 clones were sequenced using Sanger sequencing (Baseclear, the Netherlands). The first and last 100 bp were removed using CodonCode aligner, as sequence quality was insufficient in these regions. Qiime processing was performed on the sequences as described above using a similarity criterium >99% which is defined to be the minimum similarity between species (Janda and Abbott 2007). BLASTn was used to retrieve the identity of each species, and BLAST results with the same species but a different strain were grouped together for phylogenetic resolution at species level. The closest relates strain was then used to retrieve genomic information. Sequences obtained are deposited under the BioProject accession number PRJNA505600 (raw merged amplicon reads) and MK185473 – MK185614 (1450 bp 16S genes) in the NCBI database. Cell fixation and fluorescence *in situ* hybridisation (FISH) were carried out as described by Johnson et al. (2009) using the probes listed in table S2, except that hybridization was carried out overnight. Additionally, DAPI staining was used to stain all microbial

cells by incubating the multi-wells microscopy slides of fixed cells with 10 µL of a solution of 10 mg DAPI mL^{-1} per well for 15 min. The samples were analysed using an epifluorescence microscope (Axioplan 2, Zeiss, Germany). Digital images were acquired using a Zeiss MRM camera together with Zeiss imaging software (AxioVision version 4.7, Zeiss, Germany). The 1000x magnified images were improved by setting the 1x sharpening. Three images were taken at 400x and exported as TIFF and used for quantification of the cell surface using the QUIPS feature in Leica QWin V3 (Leica, Germany).

Modelling of the cycle analysis

To obtain the q_s^{max} and μ^{max} for the CSTRs from the cycle analysis, a model was constructed. Herbert-Pirt relation for substrate uptake was simplified by neglecting maintenance, as maintenance is not measured and is assumed to be a small contribution compared to q_s^{max}:

$$\mu = Y_{xs} \cdot q_s \qquad (1.1)$$

Monod kinetics were used to describe the growth rate as a function of the substrate concentration at a value of 0.1 mmol L^{-1} of either xylose or glucose:

$$\mu = \mu^{max} \cdot \frac{C_s}{C_s + K_s} \qquad (1.2)$$

The model estimated C_s and C_x by varying the biomass and substrate concentration at the start of the cycle analysis ($C_{x,0}$, $C_{s,0}$) and Y_{xs} and q_s^{max} values giving the best

fit, and a boundary value of μ is zero was applied when C_s was zero. The modelled values were then optimised to the measured data with a minimisation of the sum-squared error, using the non-linear solver in Microsoft Excel (2010).

Analysis of on-line data collected from the bioreactors

For SBRs, the μ^{max} was calculated per cycle using the recorded base dosage values. Microbial growth was directly correlated to the base consumption due to acid production in fermentation (Figure S3). A script was developed in Matlab (version 2014, USA), further explained in the supplementary information (SI) section.

COD and carbon balances

During steady state carbon and chemical oxygen demand (COD) balances were set up using the elemental matrix given in table S4. COD and carbon balances were set up by multiplying the values in the table 9 with the in- and outgoing rates in the reactor, while the NADH, ATP and Gibbs energy balances were set up by multiplying the values in table 9 with the yield on glucose. Data reconciliation was used to obtain closed balances for H, C, O, N and charge using the method described by van der Heijden *et al.* (1994). These balances were used to calculate the Gibbs energy of dissipation.

Carbon and COD balances were set up for the cycle analyses by subtracting the amount of carbon or COD in the compounds measured at a time in the cycle from the measured available carbon or COD at the start of the cycle.

Results

Xylose and glucose fermentation product spectra are similar in SBRs and different in CSTRs

Four different enrichment reactors were operated and analysed for their main products in liquid and gas phase after steady-state was established; this was obtained after 20 SRTs for all enrichments. The glucose SBR exhibited the largest shift in product spectrum during the adaptation, as initially acetate and propionate were the dominant products which changed to acetate and ethanol as dominant products after 18 SRTs. The product spectrum in the xylose and glucose SBR enrichments was very similar, dominated by a catabolic reaction producing ethanol and acetate (Figure 2A), coupled with hydrogen and formate production (Figure 1). Regarding the by-products formed, the xylose SBR enrichment produced more succinate, while the glucose SBR enrichment produced more propionate and lactate.

The xylose CSTR enrichment also had a product spectrum dominated by acetate and ethanol (Figure 2B), coupled to the production of hydrogen and formate. In the glucose CSTR, butyrate was a dominant product, followed by acetate and ethanol (Figure 2B). Both these catabolic pathways were coupled with hydrogen and formate production. Regarding the by-products, similar to the SBRs, the glucose CSTR enrichment produced more propionate and lactate, while the xylose CSTR enrichment produced more succinate, with a significant yield of succinate production in this enrichment of 0.09 Cmol $Cmol_S^{-1}$ succinate formed.

Summing up, the glucose SBR and the xylose SBR and CSTR enrichment displayed similar product spectra dominated by acetate and ethanol, while the glucose CSTR showed a mixed product spectrum of butyrate, acetate and ethanol. Glycerol was not detected in a significant amount in any of the enrichments. which was detected up to 0.1 Cmol $Cmol_S^{-1}$ by Temudo et al. (2009).

Carbon and COD balances were nearly closed in all enrichments

For all enrichments the carbon and chemical oxygen demand (COD, *i.e.*, electron) balances could be closed from the measured products at 95% and 105%, respectively (Table S3). Only in the glucose SBR enrichment a significant amount of 10% of carbon and COD could not be recovered in the outflows of the reactor. A characteristic peak at a retention time of 19.1 min was present on the HPLC UV channel for the glucose SBR which could not be identified but was confirmed to be neither 1,3-propanediol nor malate, fumarate, 2,3-butanediol, acetoin or hydroxyvalerate.

No storage response or sequential fermentation during cycle analysis

For all four enrichments a pulse experiment was performed, in which the substrate and products were measured in time and used to set up a carbon and COD balance over the cycle. A typical storage response would show COD “disappearing” during the initial fermentation phase until the substrate is depleted, while it reappears after substrate depletion as formed products. No such response was observed in both the

CSTR and SBR enrichments (Figure S2) and no sequential conversion of intermediate fermentation products was detected in the cycle analysis in SBRs (Figure S3).

Fast kinetics for SBR enrichments and high biomass yield for CSTR enrichment

At steady state, the yield of biomass formation on substrate was determined in all four enrichments (Table 1). There was no significant difference in biomass yield between the glucose CSTR enrichment reported here and by Temudo *et al.* (2009). The xylose CSTR enrichment displayed a 43% lower biomass yield than the glucose CSTR, and a 25% lower value compared to the xylose CSTR enrichment reported by Temudo et al. 2009. The glucose SBR, the xylose SBR and the xylose CSTR enrichment showed similar biomass yield values.

Through analysis of the on-line fermentation data the μ^{max}-value for each fermentation cycle could be determined for the SBR enrichments (see SI, figure S5 and S6). A cycle analysis in the CSTR enrichment cultures was used to estimate q_s^{max}. The actual q_s-value in the xylose CSTR enrichment was 1.06 $Cmol_S\ Cmol_X^{-1}\ h^{-1}$, which was 38% lower than the measured q_s^{max}. The actual q_s^{max}-value in the glucose CSTR enrichment was 0.55 $Cmol_S\ Cmol_X^{-1}\ h^{-1}$ which was 48% lower than the maximal rate of glucose uptake. The xylose CSTR enrichment exhibited a 62% higher q_s^{max}-value than the glucose CSTR enrichment. The q_s^{max} value found for the xylose SBR enrichment was statistically significantly lower (33%) than for the glucose SBR enrichment (Table 1, $p = 0.002$).

Microbial community analyses highlighted higher diversity with xylose

Amplicon sequencing of the V3-V4 region of the 16S rRNA gene was used to obtain a relative snapshot of the dynamics of the community over time. Then, FISH analysis with three different probes targeting the 16S rRNA of populations of the genus *Clostridium* and of the families of *Enterobacteriaceae* or *Lachnospiraceae* was used to analyse the microbial communities in the enrichments. Lastly, clone libraries were created of the full 16S gene to obtain species-level information of the communities. Microbial diversity was evaluated by the abundance and number of families or genera present.

The xylose SBR enrichment was dominated by *Enterobacteriaceae* (Figure 3, Table 2, figure S7) and a side population of *Lachnospiraceae* and *Clostridium* (Table 2). The 16S amplicon sequencing revealed that the *Enterobacteriaceae* were dominated by *Citrobacter* species (Figure 3), which was confirmed to be *Citrobacter freundii* using the clone library (Figure 4).

The glucose SBR enrichment was dominated by *Enterobacteriaceae* (Figure 3, Table 2, figure S7) with a side population of *Lachnospiraceae*. The 16S amplicon sequencing shows that the *Enterobacteriaceae* were dominated by *Enterobacter* species (Figure 3), which is confirmed to be *Enterobacter cloacae* by the clone library (Figure 4). Two other species also were confirmed using the clone library, *Raoultella ornithinolytica* and *Citrobacter freundii*. Thus, both SBR enrichments were dominated

by a single *Enterobacteriaceae* species, with side-populations of *Lachnospiraceae* in both SBRs, and *Clostridium* in the xylose SBR enrichment.

The glucose CSTR enrichment is dominated by *Clostridium* species (Figure 3, Table 2, figure S7) with a side population of *Enterobacteriaceae* (Table 2). The 16S amplicon sequencing gave two main OTUs, an *Enterobacter* sp. and *Clostridium* sp. (Figure 3), which are confirmed to be *Clostridium intestinale* and *Raoultella ornithinolytica*.

The xylose CSTR enrichment is dominated by *Lachnospiraceae* and *Enterobacteriaceae* species (Figure 3, Table 2, figure S7). The 16S amplicon sequencing is dominated by a Citrobacter sp., while two OTUs from the *Lachnospiraceae* are present. The clone library reveals that the *Citrobacter* OTU corresponds to *Citrobacter freundii*, while only one of the *Lachnospiraceae* OTUs can be confirmed up to family level, as it only shows 96% sequence similarity with the closest cultivated relative *Lachnotalea glycerinii* (Table S6).

Summing up, it can be argued that the glucose SBR and CSTR enrichment showed a similar level of diversity, with a dominant species and a small side-population. The xylose SBR enrichment was more diverse than the glucose enrichments, as the side population contains both *Clostridium* and *Lachnospiraceae* species. In the xylose CSTR the largest diversity was observed, as here *Citrobacter freundii*, an uncultivated *Lachnospiraceae* species and a *Muricomes* population dominated.

Discussion

Pathway analysis of the enrichments

Under slightly alkaline and mesophilic conditions acetate and ethanol were the dominant products under SBR conditions, while butyrate formation occurred significantly under CSTR conditions. Compared to the work of Temudo *et al.* (2009) we observe a similar product spectrum in the glucose CSTR enrichment, though we observe more ethanol and less butyrate. The xylose CSTR enrichment is dominated by acetate and ethanol, while the enrichment of Temudo *et al.* (2009) had produced primarily butyrate and acetate. Acetate and ethanol have been shown as the dominant products at pH 7.9 and 30°C (Zoetemeyer, van den Heuvel and Cohen 1982), while acetate and butyrate have been dominant products under at pH 7.0 and 36°C (Fang and Liu 2002).

The rate of the supply of inert N_2 gas in the reactor broth was the only difference in experimental procedures between the present study and the work of Temudo *et al.* (2009). This could potentially change the hydrogen and carbon dioxide gas partial pressures. The impact of the gas flow rate on the fermentation pattern was investigated, in order to investigate if the gas flow rate could explain the differences in product spectrum observed. Little effect was found on all product yields and hydrogen partial pressure (Figure S1); thus, we expect no major impact of the gas flow rate. Furthermore, the glucose CSTR enrichment was duplicated and the resulting product spectrum of both enrichments was identical (Figure S1) which confirms the reproducibility of the enrichments.

A NADH balance was set up using the generalised metabolic network (Figure 1, Table S4), and the derivates from the pyruvate to acetyl-CoA pathway were summed as a yield. The NADH balance of the four enrichments shows that the glucose CSTR has a small net producing NADH balance, whereas the two SBRs and the xylose CSTR have a small net NADH consuming balance. Minor discrepancies from the NADH-balance can possibly be explained by succinate production through an NADH producing pathway, such as through the oxidative branch of the TCA cycle. Assuming no net NADH consumption for succinate production would bring the two SBRs and the xylose CSTR to a closed NADH balance.

Comparable values for the acetyl-CoA derivates and H_2/formate production (Table 3) indicate that H_2/formate production is directly coupled to pyruvate conversion to acetyl-CoA in the metabolic network as in Figure 1. Only for the xylose CSTR enrichment there is significantly less formate and H_2 found than acetyl-CoA derivates, which suggest that H_2 and formate are consumed through homoacetogenesis as proposed by (Regueira *et al.* 2018).

The stoichiometric data argues for the PPP to be active in the xylose SBR, as acetate and ethanol are present in equimolar amounts and there is no excess of acetyl-CoA derivates compared to formate/H_2. If the PKP would have been active, more acetate compared to ethanol would have been expected and less acetyl-CoA derivates compared to formate/H_2. In *Clostridium acetobutylicum* the PKP has been significantly expressed under batch cultivation (Liu *et al.* 2012), but here the PPP is assumed to be the only pathway active under SBR conditions.

Bioenergetics and the role of substrate uptake

Using the metabolic network (Figure 1) the amount of ATP produced was estimated from the different catabolic products ($Y_{ATP,s}$). Combining this yield with the biomass yield, the biomass yield on ATP ($Y_{x,ATP}$) was calculated. The $Y_{x,ATP}$ values for the xylose SBR and CSTR are very similar (Table 4), while the $Y_{x,ATP}$ values for the glucose SBR and CSTR enrichments are higher (Table 4). $Y_{x,ATP}$ values are confirmed by the dissipation energy, as the xylose SBR and CSTR enrichment show a similar value, while the value for the glucose SBR enrichment is higher and the highest value is reported for the glucose CSTR enrichment. This means the xylose enrichments have a considerably lower energetic efficiency than the glucose enrichments. The dissipation values obtained for glucose is in accordance with the average values for glucose (-236 kJ $Cmol_x^{-1}$) , while that of xylose is considerably higher than according to the correlation function (-246 kJ $Cmol_x^{-1}$) (Heijnen, van Loosdrecht and Tijhuis 1992).

The higher dissipation in the xylose enrichments can be caused by the cost of transporting xylose over the cell membrane. Xylose can be taken up into the cell by two different mechanisms. XylE is an enzyme which uses the proton motive force to take up xylose from the surrounding medium, through the symport with one proton (Davis and Henderson 1987). When assuming a stoichiometry of 2.67 mol H^+ per mol ATP used, this means xylose uptake XylE costs 0.375 mol ATP per mol xylose. A second method for active xylose uptake is via XylFGH, an ATP-binding cassette (ABC) transporter which uses the direct dephosphorylation of ATP to import xylose (Sumiya *et al.* 1995). XylE is known to be a low affinity transporter, while XylFGH is a

high affinity transporter (Sumiya *et al.* 1995). In *E. coli* it has been demonstrated that in batch conditions XylE plays a minor role in xylose uptake (Hasona *et al.* 2004).

The genome of the strain with the highest similarity was assessed for the presence of transporters. *Citrobacter freundii* strain P10159 dominant in the xylose SBR enrichment (Table S6) contains the XylE gene and not the analogues XylF, XylG or XylH (accession number CP012554.1) This argues for the nature of XylE as a high-rate xylose transport enzyme. A different *Citrobacter freundii* strain FDAARGOS (accession number CP026056.1) was populating the xylose CSTR, which contained neither XylE nor XylF, XylG or XylH. This suggests novel ABC transporters might be present in the xylose CSTR population.

Glucose uptake can be more energy efficient. The phosphotransferase system (PTS) is an uptake mechanism which couples the transfer of a phosphate group from PEP to glucose to transport glucose over the membrane, thus there is no net ATP cost for importing glucose as glucose-phosphate is directly produced. This complex is assumed to be active in both SBR and CSTR as this is observed to be the main transport system under glucose excess (Steinsiek and Bettenbrock 2012) and under substrate limitation (Babu *et al.* 2005). The *Enterobacter cloacae* strain AA4 dominant in the glucose SBR enrichment and the *Clostridium intestinale* strain URNW dominant in the glucose CSTR enrichment both contain all five genes necessary to express the PTS complex in their genomes (accession number CP018785.1 and HM801879.1).

When incorporating this biochemical consideration for substrate uptake, the $Y_{x,ATP}$ value for xylose and glucose becomes similar (Table 4), while the 50% difference in $Y_{X,ATP}$ between SBR and CSTR enrichments remains.

Xylose uptake is slower than glucose uptake in SBR

When substrate is only used for growth and no storage products are formed, the competition in a SBR process is based on the μ^{max} of the competing microorganisms, which can be maximised through $Y_{x,s}$ or q_s^{max}. The SBR grown cultures described in this paper are optimized for q_s^{max} (Table 1). The q_s^{max} of the glucose SBR enrichment is 50% higher than the xylose SBR enrichment. The lower uptake rate for xylose can be explained by a kinetic bottleneck identified in the PPP. Gonzalez *et al.* (2017) have shown that in glycolysis *E. coli* metabolises glucose to fructose-6-phosphate at a rate of 90 mmol g_{DW}^{-1} h^{-1}, while in the PPP rates to form fructose-6-phosphate did not exceed 37 mmol g_{DW}^{-1} h^{-1}. The production of formate, acetate and ethanol exceeded these values for glucose, indicating the lower part of fermentation was not rate limiting.

Acetate and ethanol production as a kinetic advantage

The q_s^{max} and μ^{max} for the CSTR grown glucose enrichment producing butyrate is significantly lower than the acetate and ethanol producing enrichment (Table 1 and Temudo et al. 2009). Furthermore, the xylose CSTR enrichment of Temudo *et al.* (2009) and the glucose CSTR enrichment performed here, showed a similar q_s^{max}-value (Table 1) and both enrichments are producing a significant amount of butyrate.

On top of that, both SBRs produce dominantly acetate and ethanol, where q_s^{max} is a more important competitive advantage than in CSTR conditions. The kinetic difference between butyrate forming and acetate and ethanol forming microorganisms is observed in pure cultures. The μ^{max} of *Clostridium tyrobutyricum*, a butyrate producer, is 0.12 h^{-1} (Liu and Yang 2006) and *Citrobacter* sp. CMC-1, an acetate and ethanol producer, is 0.21 h^{-1} (Mangayil, Santala and Karp 2011) grown under similar conditions. The fact that acetate and ethanol formation is related to higher μ^{max} is also indirectly shown by the study of Zoetemeyer *et al.* (1982), as a μ of 0.25 h^{-1} was applied here at pH 7.9 and 30°C obtaining a product spectrum of acetate and ethanol, while Temudo *et al.* (2009) and this study obtain also butyrate production at a μ of 0.13 h^{-1}. This kinetic advantage seems to hold only for fermentations at pH higher than 6.25, as enrichments performed in CSTR mode at pH 5.5 above μ^{max} have demonstrated to systemically yield a product spectrum dominated by acetate, butyrate, and lactate (Rafrafi *et al.* 2013). This kinetic effect can be incorporated into model-based evaluation of mixed culture fermentations to improve the prediction of butyrate, acetate and ethanol production at neutral and alkaline pH.

Butyrate production as an efficient pathway

If acetate and ethanol production obtains a higher q_s^{max} value than butyrate, and both pathways produce 3 mol ATP, there seems to be no advantage for butyrate production over acetate and ethanol production. Thermodynamically, butyrate formation yields more energy than acetate and ethanol production, (-264 kJ mol^{-1} and -226 kJ mol^{-1} respectively). This energy is available in the step from crotonyl-CoA to

599 butyryl-CoA, which is calculated to be -50 kJ/mol (González-Cabaleiro, Lema and
600 Rodríguez 2015). A direct conversion of this energy into a proton motive force has
601 been rejected (Herrmann *et al.* 2008). Part of the energy can be conserved by
602 coupling this energy to the transfer of the electrons from NADH to ferredoxin and
603 then oxidizing ferredoxin with NAD^+ to generate a sodium motive force using the Rnf
604 enzyme (Herrmann *et al.* 2008). Two of the six subunits of this complex are found in
605 the genome of the *Clostridium intestinale* strain URNW, indicating the possibility of
606 this mechanism being active in the glucose CSTR enrichment.
607
608 **Metabolic strategies in fermentation: r-organisms vs K-organisms**
609
610 The CSTR enrichments, when corrected for substrate uptake, show about 50%
611 higher $Y_{x,ATP}$ value than the SBR enrichments. The q_s^{max}-value on the other hand is
612 2-3 times higher for the SBR enrichments compared to the CSTR enrichments.
613 These observations correspond with the general microbial theory proposed on r- vs
614 K-organisms (Andrews and Harris 1986). The r-organisms are more adapted to a
615 substrate-abundant environment and display high q_s^{max} and μ^{max} values. K-organisms
616 are more adapted to crowded environment where substrate is limited and display
617 high $Y_{x,ATP}$ and K_s values. The reason r-organisms dissipate more energy than K-
618 organisms in their metabolism may rely on the fact that at increasing growth rate
619 more erroneous proteins are produced due to a higher error rate made during
620 proofreading at higher speed (Yamane *et al.* 1977). Thus, more non-functional
621 proteins are produced at higher growth rate. As protein production is estimated to
622 cost >80% of the ATP to synthesise a cell (Hespell and Bryant 1979), larger error

623 rates will cause increased ATP cost per cell assuming a similar functioning protein
624 content.
625
626 The community data shows that *Enterobacteriaceae* dominate the SBR
627 environments, thus the *Citrobacter freundii* and *Enterobacter cloacae* species can be
628 classified as r-organisms. *Enterobacteriaceae* species such as *E. coli* are well known
629 to exhibit high growth rates in anaerobic environments with carbohydrates (De Vrije
630 and Claassen 2003). *Clostridium* species on the other hand are often dominating in
631 substrate-limited environments such as anaerobic digesters (Burrell *et al.* 2004),
632 where the rate of hydrolysis of cellulose and hemicellulose is an order of magnitude
633 lower than typical fermentation rates, creating a substrate-limited environment. In the
634 glucose CSTR we observe a dominance of *Clostridium intestinale*, which fits with
635 these observations.
636
637 **The microbial community composition and the effect of limiting a single**
638 **substrate**
639
640 First of all, it is noteworthy that the FISH imaging and the 16S rRNA gene amplicon
641 sequencing data do not always correspond. In the glucose SBR, the dominance of
642 *Enterobacteriaceae* on OTU-level is confirmed by the FISH analysis, but in the
643 glucose CSTR enrichment the *Enterobacteriaceae* are observed to be a minor
644 fraction on cell-level (FISH image), while 30% of the reads relate to
645 *Enterobacteriaceae*. In the xylose CSTR a similar bias is observed, as 53% of the
646 community is identified as *Lachnospiraceae* using FISH (Table 2), while only 15% of
647 the reads relate to *Lachnospiraceae*. As we have corrected the data for copy

numbers, the bias is likely caused by DNA extraction and PCR biases, which are known to cause biases in amplicon sequencing data (Brooks *et al.* 2015). As proposed by Amann, Ludwig and Schleifer (1995), 16S rRNA gene sequencing and FISH analysis have to be used in parallel to obtain an accurate estimation of the microbial community structure, which is confirmed in the study here.

Here, populations of *Enterobacteriaceae*, *Lachnospiraceae* and *Clostridium* dominated the enrichments. *Clostridium* and *Enterobacteriaceae* populations have been reported in enrichments on mineral medium (Table 5), though for the first time *Lachnospiraceae* were enriched on xylose. We find that a significant presence of *Clostridium* was linked to butyrate production, as in the glucose CSTR, which is confirmed by other enrichment studies (Table 5). The butyryl-CoA dehydrogenase gene, which is responsible for the reduction of crotonyl-CoA to butyryl-CoA using NADH, is found in organisms in the *Clostridium* species, while neither in *Enterobacter* nor in *Citrobacter* species according to the NCBI Gene database.

The glucose enrichments seem to be dominated by a single species with one side populating family, which is *Enterobacter cloacae* in the glucose SBR and *Clostridium intestinale* in the glucose CSTR. It was expected that, when limiting a single substrate, one specialist will dominate the community after prolonged cultivation, displaying either the highest μ^{max} or the highest affinity. For the xylose enrichments, the communities are more diverse. In the xylose SBR, *Citrobacter freundii* dominated the culture, with a side-population of both, *Lachnospiraceae* and *Clostridium*. The xylose CSTR is populated by two *Lachnospiraceae* OTUs (Figure 3), one of which is confirmed to be an uncultivated *Lachnospiraceae* species (Table S6) next to a

673 population of *Citrobacter freundii*. Thus, xylose fermentation results in more microbial
674 diversity than glucose fermentation.
675
676 All four enrichments are populated by more than one species, with stabilizing OTUs
677 over time (Figure 3). This indicates that species have a reason to coexist in these
678 single substrate limited systems. It is possible that mutualistic relationships between
679 these species are present, *e.g.*, in the form of a B-vitamin exchange between species
680 (Magnúsdóttir *et al.* 2015), as these communities are cultivated on mineral medium.
681 Overall, it remains an important ecological question why in many cases rather diverse
682 communities remain in very selective conditions with one limiting substrate.
683
684 Overall, this study aimed to show the impact of sequencing batch and continuous
685 culturing on microbial communities fermenting lignocellulosic sugars such as xylose
686 and glucose. Butyrate formation was linked to slow uptake rate, while acetate and
687 ethanol formation was linked to high uptake rates. This kinetic effect can be taken
688 into account in modelling efforts. In SBR, xylose was fermented 33% slower than
689 glucose. SBR communities maximised their q_s^{max}, while CSTR communities
690 maximised their $Y_{x,ATP}$. SBR communities were dominated by r-strategists like
691 *Citrobacter freundii* and *Enterobacter cloacae*, and the CSTR communities by K-
692 organisms like *Clostridium intestinale* and *Lachnospiraceae* species. No significant
693 storage of either xylose or glucose was observed in the SBR enrichments. The
694 glucose enrichments confirmed the hypothesis that limitation of a single substrate
695 leads to domination of a single species. The xylose enrichments displayed more
696 microbial diversity, with the xylose CSTR up to three dominant populations.
697

Acknowledgements

The authors wish to thank Cor Ras and Max Zomerdijk for technical assistance in analytics, Ben Abbas for help with the clone libraries and sequencing, Lars Puiman for his help in improving the FISH hybridisation for Gram+ microorganisms and Rebecca Gonzalez-Cabaleiro at Newcastle University for discussion on metabolic strategies in fermentations. This work was supported by the Soenghen Institute for Anaerobic Microbiology (SIAM), SIAM gravitation grant, the Netherlands Organization for Scientific Research (024.002.002).

References

Amann RI, Ludwig W, Schleifer KH. Phylogenetic identification and in situ detection of individual microbial cells without cultivation. *Microbiol Rev* 1995;**59**:143–69.

Andrews JH, Harris RF. r- and K-Selection and Microbial Ecology. In: Marshall KC (ed.). *Advances in Microbial Ecology*. Boston, MA: Springer US, 1986, 99–147.

Anwar Z, Gulfraz M, Irshad M. Agro-industrial lignocellulosic biomass a key to unlock the future bio-energy: A brief review. *J Radiat Res Appl Sci* 2014;**7**:163–73.

APHA. *Standard Methods for the Examination of Water and Wastewater*. 20th ed. Washington D.C.: American Public Health Association, 1998.

Babu R, M.P. N, Vignesh M *et al.* Proteome analysis to assess physiological changes in Escherichia coli grown under glucose- limited fed- batch conditions. *Biotechnol Bioeng* 2005;**92**:384–92.

Beijerinck M. Anhaufungsversuche mit Ureumbakterien. *Cent f Bakteriol* 1901;**7**:33–61.

Brooks JP, Edwards DJ, Harwich MD *et al.* The truth about metagenomics:

Quantifying and counteracting bias in 16S rRNA studies Ecological and evolutionary microbiology. *BMC Microbiol* 2015;**15**:1–14.

Buckel W, Thauer RK. Energy conservation via electron bifurcating ferredoxin reduction and proton/Na+ translocating ferredoxin oxidation. *Biochim Biophys Acta - Bioenerg* 2013;**1827**:94–113.

Burrell PC, O'Sullivan C, Song H *et al.* Identification, Detection, and Spatial Resolution of Clostridium Populations Responsible for Cellulose Degradation in a Methanogenic Landfill Leachate Bioreactor. *Appl Environ Microbiol* 2004;**70**:2414–9.

Caporaso JG, Kuczynski J, Stombaugh J *et al.* QIIME allows analysis of high-throughput community sequencing data. *Nat Methods* 2010;**7**:335.

Chunfeng C, Yoshitaka E, Yuhei I *et al.* Effect of hydraulic retention time on the hydrogen yield and population of Clostridium in hydrogen fermentation of glucose. *J Environ Sci* 2009;**21**:424–8.

Davis EO, Henderson PJ. The cloning and DNA sequence of the gene xylE for xylose-proton symport in Escherichia coli K12. *J Biol Chem* 1987;**262**:13928–32.

DeSantis TZ, Hugenholtz P, Larsen N *et al.* Greengenes, a Chimera-Checked 16S rRNA Gene Database and Workbench Compatible with ARB. *Appl Environ Microbiol* 2006;**72**:5069–72.

Fang HHP, Liu H. Effect of pH on hydrogen production from glucose by a mixed culture. *Bioresour Technol* 2002;**82**:87–93.

Ghisellini P, Cialani C, Ulgiati S. A review on circular economy: the expected transition to a balanced interplay of environmental and economic systems. *J Clean Prod* 2016;**114**:11–32.

748 González-Cabaleiro R, Lema JM, Rodríguez J. Metabolic Energy-Based Modelling
749 Explains Product Yielding in Anaerobic Mixed Culture Fermentations. *PLoS One*
750 2015;**10**:1–17.
751 Gonzalez JE, Long CP, Antoniewicz MR. Comprehensive analysis of glucose and
752 xylose metabolism in Escherichia coli under aerobic and anaerobic conditions by
753 13C metabolic flux analysis. *Metab Eng* 2017;**39**:9–18.
754 Hasona A, Kim Y, Healy FG *et al.* Pyruvate Formate Lyase and Acetate Kinase Are
755 Essential for Anaerobic Growth of Escherichia coli on Xylose. *J Bacteriol*
756 2004;**186**:7593–600.
757 van der Heijden RTJM, Heijnen JJ, Hellinga C *et al.* Linear constraint relations in
758 biochemical reaction systems: I. Classification of the calculability and the
759 balanceability of conversion rates. *Biotechnol Bioeng* 1994;**43**:3–10.
760 Heijnen JJ, van Loosdrecht MCM, Tijhuis L. A black box mathematical model to
761 calculate auto- and heterotrophic biomass yields based on Gibbs energy
762 dissipation. *Biotechnol Bioeng* 1992;**40**:1139–54.
763 Herrmann G, Jayamani E, Mai G *et al.* Energy Conservation via Electron-Transferring
764 Flavoprotein in Anaerobic Bacteria. *J Bacteriol* 2008;**190**:784–91.
765 Hespell RB, Bryant MP. Efficiency of Rumen Microbial Growth: Influence of some
766 Theoretical and Experimental Factors on YATP. *J Anim Sci* 1979;**49**:1640–59.
767 Janda JM, Abbott SL. 16S rRNA Gene Sequencing for Bacterial Identification in the
768 Diagnostic Laboratory: Pluses, Perils, and Pitfalls. *J Clin Microbiol*
769 2007;**45**:2761–4.
770 Jia H-R, Geng L-L, Li Y-H *et al.* The effects of Bt Cry1Ie toxin on bacterial diversity in
771 the midgut of Apis mellifera ligustica (Hymenoptera: Apidae). *Sci Rep*
772 2016;**6**:24664.

773 Johnson K, Jiang Y, Kleerebezem R *et al.* Enrichment of a Mixed Bacterial Culture
774 with a High Polyhydroxyalkanoate Storage Capacity. *Biomacromolecules*
775 2009;**10**:670–6.
776 Johnson M, Zaretskaya I, Raytselis Y *et al.* NCBI BLAST: a better web interface.
777 *Nucleic Acids Res* 2008;**36**:W5–9.
778 Kleerebezem R, van Loosdrecht MC. Mixed culture biotechnology for bioenergy
779 production. *Curr Opin Biotechnol* 2007;**18**:207–12.
780 de Kok S, Meijer J, van Loosdrecht MCM *et al.* Impact of dissolved hydrogen partial
781 pressure on mixed culture fermentations. *Appl Microbiol Biotechnol*
782 2013;**97**:2617–25.
783 Kuenen JG. *Continuous Cultures (Chemostats)*. Elsevier Inc., 2014.
784 Li F, Hinderberger J, Seedorf H *et al.* Coupled Ferredoxin and Crotonyl Coenzyme A
785 (CoA) Reduction with NADH Catalyzed by the Butyryl-CoA Dehydrogenase/Etf
786 Complex from Clostridium kluyveri . *J Bacteriol* 2008;**190**:843–50.
787 Lin Y, de Kreuk M, van Loosdrecht MCM *et al.* Characterization of alginate-like
788 exopolysaccharides isolated from aerobic granular sludge in pilot-plant. *Water*
789 *Res* 2010;**44**:3355–64.
790 Liu L, Zhang L, Tang W *et al.* Phosphoketolase Pathway for Xylose Catabolism in
791 Clostridium acetobutylicum Revealed by 13C Metabolic Flux Analysis. *J*
792 *Bacteriol* 2012;**194**:5413–22.
793 Liu X, Yang S-T. Kinetics of butyric acid fermentation of glucose and xylose by
794 Clostridium tyrobutyricum wild type and mutant. *Process Biochem* 2006;**41**:801–
795 8.
796 Magnúsdóttir S, Ravcheev D, de Crécy-Lagard V *et al.* Systematic genome
797 assessment of B-vitamin biosynthesis suggests co-operation among gut

798 microbes. *Front Genet* 2015;**6**:148.
799 Mangayil R, Santala V, Karp M. Fermentative hydrogen production from different
800 sugars by Citrobacter sp. CMC-1 in batch culture. *Int J Hydrogen Energy*
801 2011;**36**:15187–94.
802 Marshall CW, LaBelle E V, May HD. Production of fuels and chemicals from waste by
803 microbiomes. *Curr Opin Biotechnol* 2013;**24**:391–7.
804 Pirt SJ. The maintenance energy of bacteria in growing cultures. *Proc R Soc London*
805 *Ser B Biol Sci* 1965;**163**:224 LP-231.
806 Prakash O, Shouche Y, Jangid K *et al.* Microbial cultivation and the role of microbial
807 resource centers in the omics era. *Appl Microbiol Biotechnol* 2013;**97**:51–62.
808 Rafrafi Y, Trably E, Hamelin J *et al.* Sub-dominant bacteria as keystone species in
809 microbial communities producing bio-hydrogen. *Int J Hydrogen Energy*
810 2013;**38**:4975–85.
811 Regueira A, González-Cabaleiro R, Ofiţeru ID *et al.* Electron bifurcation mechanism
812 and homoacetogenesis explain products yields in mixed culture anaerobic
813 fermentations. *Water Res* 2018:5–13.
814 Ren NQ, Chua H, Chan SY *et al.* Assessing optimal fermentation type for bio-
815 hydrogen production in continuous-flow acidogenic reactors. *Bioresour Technol*
816 2007;**98**:1774–80.
817 Rodriguez J, Kleerebezem R, Lema JM *et al.* Modeling product formation in
818 anaerobic mixed culture fermentations. *Biotechnol Bioeng* 2006;**93**:592–606.
819 Spirito CM, Richter H, Stams AJ *et al.* Chain elongation in anaerobic reactor
820 microbiomes to recover resources from waste. *Curr Opin Biotechnol*
821 2014;**27**:115–22.
822 Steinsiek S, Bettenbrock K. Glucose Transport in Escherichia coli Mutant Strains with

Defects in Sugar Transport Systems. *J Bacteriol* 2012;**194**:5897–908.

Sumiya M, O Davis E, C Packman L *et al.* Molecular genetics of a receptor protein for D-xylose, encoded by the gene xylF in Escherichia coli. *Receptors Channels* 1995;**3**:117–28.

Temudo MF, Kleerebezem R, van Loosdrecht M. Influence of the pH on (open) mixed culture fermentation of glucose: a chemostat study. *Biotechnol Bioeng* 2007;**98**:69–79.

Temudo MF, Mato T, Kleerebezem R *et al.* Xylose anaerobic conversion by open-mixed cultures. *Appl Microbiol Biotechnol* 2009;**82**:231–9.

De Vries W, Kapteijn WMC, Van Der Beek EG *et al.* Molar Growth Yields and Fermentation Balances of Lactobacillus casei L3 in Batch Cultures and in Continuous Cultures. *Microbiology* 1970;**63**:333–45.

De Vrije T, Claassen PAM. Dark hydrogen fermentations. *Bio-methane & Bio-hydrogen* 2003:103–23.

Wang Q, Garrity GM, Tiedje JM *et al.* Naive Bayesian classifier for rapid assignment of rRNA sequences into the new bacterial taxonomy. *Appl Environ Microbiol* 2007;**73**:5261–7.

Yamane T, Hopfield JJ, Yue V *et al.* Experimental evidence for kinetic proofreading in the aminoacylation of tRNA by synthetase. *Proc Natl Acad Sci* 1977;**74**:2246–50.

Zoetemeyer RJ, Arnoldy P, Cohen A *et al.* Influence of temperature on the anaerobic acidification of glucose in a mixed culture forming part of a two-stage digestion process. *Water Res* 1982;**16**:313–21.

Zoetemeyer RJ, van den Heuvel JC, Cohen A. pH influence on Acidogenic Dissimilation of Glucose in an Anaerobic Digestor. *Water Res* 1982;**16**:303–311.

Table 1: $Y_{x,s}$ calculated on the basis of TSS/VSS measurements at steady state (n=3). For the SBRs, μ^{max} was obtained from on-line fermentation data according to appendix VI. For the CSTRs, q_s^{max} was obtained from a substrate pulse experiment and subsequent fitting the substrate concentration data, with R^2 values of 0.97 and 0.92 for xylose and glucose respectively. For the SBR σ_{qsmax} is calculated using error propagation and the covariance of the μ^{max} and $Y_{x,s}$ values. For the CSTRs σ_{qsmax} is calculated using error propagation and the covariance of the C_s and C_x measurement, while $\sigma_{\mu max}$ is calculated using error propagation and the covariance of q_s^{max} and $Y_{x,s}$.

	$Y_{x,s}$ [$Cmol_x\ Cmol_s^{-1}$]	q_s^{max} [$Cmol_s\ Cmol_x^{-1}\ h^{-1}$]	μ^{max} [h^{-1}]	Reference
Xylose SBR	0.12 ± 0.01	2.28 ± 0.10	0.28 ± 0.01	This study
Glucose SBR	0.13 ± 0.01	3.41 ± 0.24	0.45 ± 0.01	This study
Xylose CSTR	0.12 ± 0.01	1.72 ± 0.02	0.22 ± 0.01	This study
	0.16 ± 0.01	1.01	0.16	Temudo *et al.* (2009)
Glucose CSTR	0.21 ± 0.01	1.06 ± 0.02	0.22 ± 0.01	This study
	0.21 ± 0.01	NA	NA	Temudo *et al.* (2009)

Table 2: Result of the FISH quantification (n = 3), with percentages denoting relative abundances calculated from the target-probe surface area compared to EUB338 probe surface. Unidentified populations were calculated as the remaining percentage after summing up the relative abundances of the known populations. The last column shows the amount of surface probed by EUB338 compared to DAPI.

	Chis150 *vs.* EUB338	**Lac435** *vs.* EUB338	**Ent183** *vs.* EUB338	**Unidentified** *vs.* EUB338	**EUB338** *vs.* DAPI
Xylose SBR	2% ± 2%	5% ± 1%	90% ± 3%	2%	96% ± 2%
Glucose SBR	ND	3% ± 2%	91% ± 3%	6%	100% ± 7%
Xylose CSTR	ND	53% ± 3%	44% ± 6%	3%	104% ± 14%
Glucose CSTR	89% ± 12%	ND	5% ± 0%	6%	89% ± 8%

Table 3: Net NADH balance calculated using table S4. Acetyl-CoA derivates were calculated from butyrate, acetate and ethanol production through the pyruvate to acetyl-CoA pathway (Figure 1).

	Net NADH balance metabolism [$mol_{NADH}\ Cmol_S^{-1}$]	Acetyl-CoA derivates [$mol\ Cmol_S^{-1}$]	Formate + H_2 [$mol\ Cmol_S^{-1}$]
Xylose SBR	-0.03 ± 0.00	0.27 ± 0.00	0.26 ± 0.00
Glucose SBR	-0.03 ± 0.01	0.22 ± 0.00	0.23 ± 0.02
Xylose CSTR	-0.06 ± 0.01	0.27 ± 0.00	0.22 ± 0.01
Glucose CSTR	0.02 ± 0.01	0.24 ± 0.20	0.25 ± 0.01

Table 4: $Y_{x,ATP}$ is calculated by assuming ATP formation per product (Table S4), for the measured data and corrected for substrate uptake. Xylose uptake in the CSTR is assumed by the XylFGH complex and the XylE complex in the SBR. Gibbs energy of dissipation is calculated at 30°C and pH = 8 using the reconciled data.

	Y_{xs} [$Cmol_X\ Cmol_S^{-1}$]	$Y_{ATP,s}$ [$mol_{ATP}\ Cmol_S^{-1}$]	$Y_{x,ATP}$ observed [$g_X\ mol^{-1}$ ATP]	$Y_{x,ATP}$ corrected [$g_X\ mol^{-1}$ ATP]	Gibbs energy of dissipation [$kJ\ Cmol_X^{-1}$]
Xylose SBR	0.12 ± 0.01	0.42 ± 0.01	7.2	8.7	-378
Glucose SBR	0.13 ± 0.01	0.40 ± 0.01	8.2[1]	8.2[1]	-285
Xylose CSTR	0.12 ± 0.01	0.42 ± 0.01	6.8	12.8	-386
Glucose CSTR	0.21 ± 0.01	0.49 ± 0.03	13.4	13.4	-236

[1]Only 90% of glucose conversion is assumed here, as the COD and carbon balance only close for 90%

874 Table 5: Reported predominant bacterial species for fermentative microbial communities
875 enriched on xylose or glucose as carbon sources in CSTR mode. Species were detected
876 using PCR and denaturing gradient gel electrophoresis or PCR and single strand
877 conformation polymorphism analysis

Substrate	**Inoculum**	**T**	**pH range**	**Dominant carbon products**	**Organisms**	**Source**
Xylose	Hot spring culture	45˚C	5.1	Acetate, butyrate	*Clostridium acetobutylicum* *Citrobacter freundii*	(Mäkinen, Nissilä and Puhakka 2012)
Xylose	Hot spring culture	37˚C	5.1	Acetate, butyrate, ethanol	*Clostridum acetobutylicum* *Clostridium tyrobutircum*	(Mäkinen, Nissilä and Puhakka 2012)
Glucose	Hot spring culture	37 ˚C	5.0	Acetate, butyrate	3 species of *Clostridium* 2 uncultured	(Karadag and Puhakka 2010)
Glucose	Activated sludge, cassava, rabbit droppings	37 ˚C	5.5	Butyrate, acetate, lactate*	*Clostridium pasteurianum,* *Clostridium beijerinckii,* *Lactobacillus paracasei*	(Rafrafi *et al.* 2013)
Xylose 4 g/L	Digestor sludge and acidification tank	30 ˚C	8.0	Acetate, butyrate	*Clostridium beijerinckii,* *Clostridium xylanovorans,* *Clostrdium sp. CCUG*	(Temudo *et al.* 2008)
Xylose	Digestor	30 ˚C	8.0	Acetate,	*Citrobacter farmeri*	(Temudo *et*

11 g/L	sludge and acidification tank			butyrate, ethanol	*Clostridium intestinale* *Clostrdium sp. CCUG*	*al.* 2008)
Glucose	Digestor sludge and acidification tank	30 ˚C	8.0	Acetate, butyrate, ethanol	*Clostridium quinii***	(Temudo *et al.* 2008)

878 * 50% of the COD coming out of the reactor was glucose

879 ** two other bands are visible which are not mentioned

880

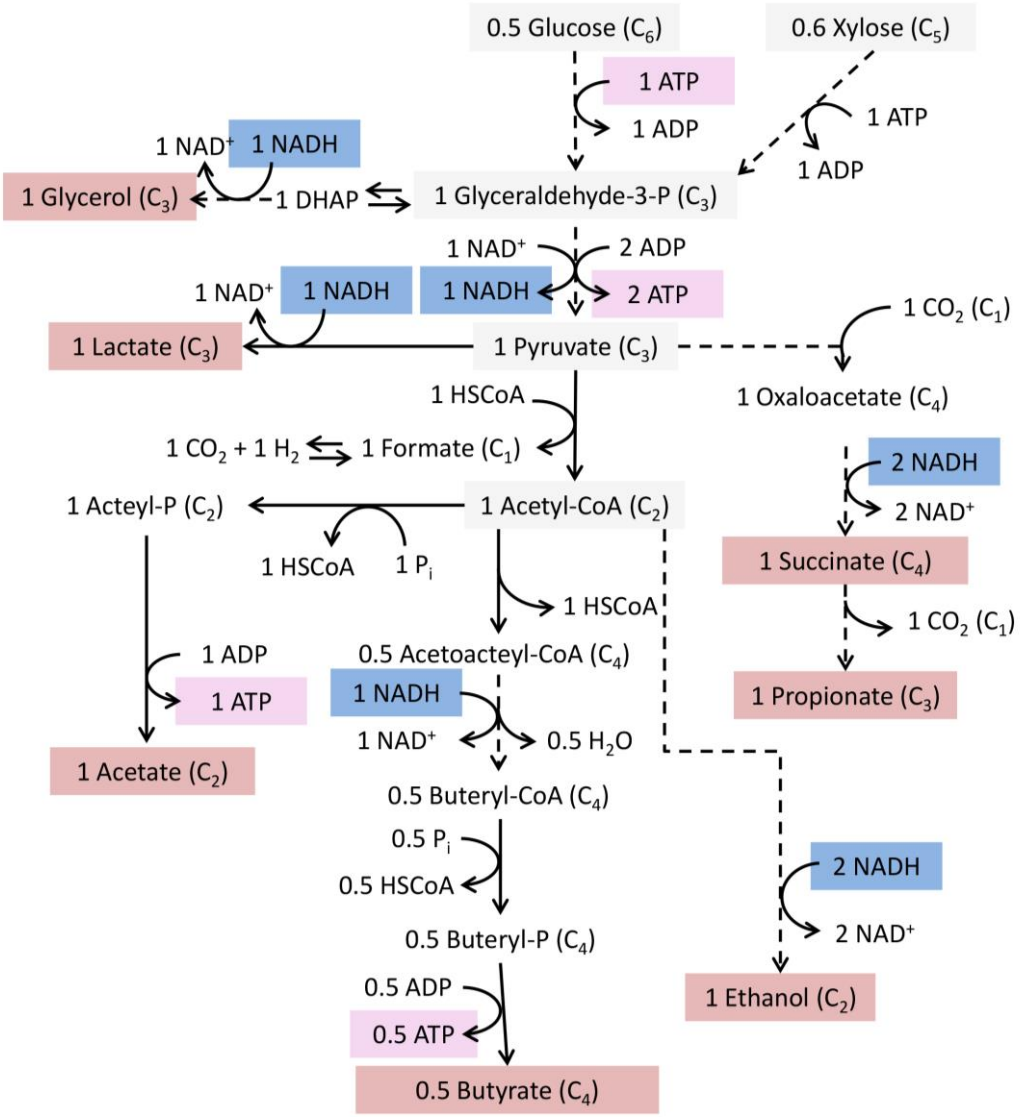

881

882 Figure 1: Intracellular metabolic network for xylose and glucose fermentations. Dashed lines
883 indicate lumped reactions, straight lines indicate single reactions. Xylose comes into the
884 glycolysis through the synthesis of 2 fructose-6-phosphate and 1 glyceraldehyde-3-
885 phosphate, through the PPP. The Emden-Meyerhof-Parnass pathway is used as this is the
886 common type of glycolysis encountered in energy limited anaerobes (Flamholz *et al.* 2013).
887 Figure is made on the basis of Madigan and Martinko (2006).

888

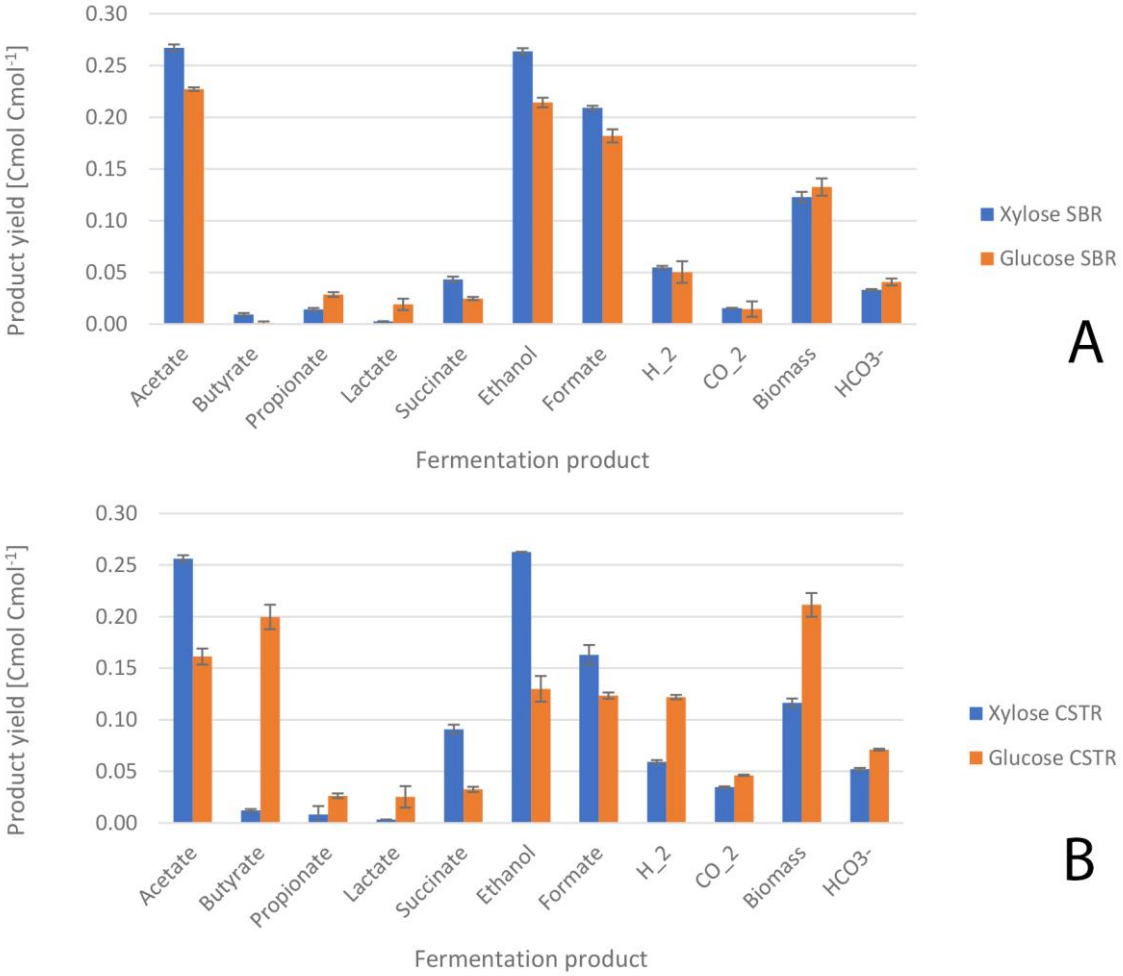

889

890

891 Figure 2: Product spectra of mixed culture fermentations of SBRs (A) and CSTRs (B)

892 determined in steady state (n=3)

893

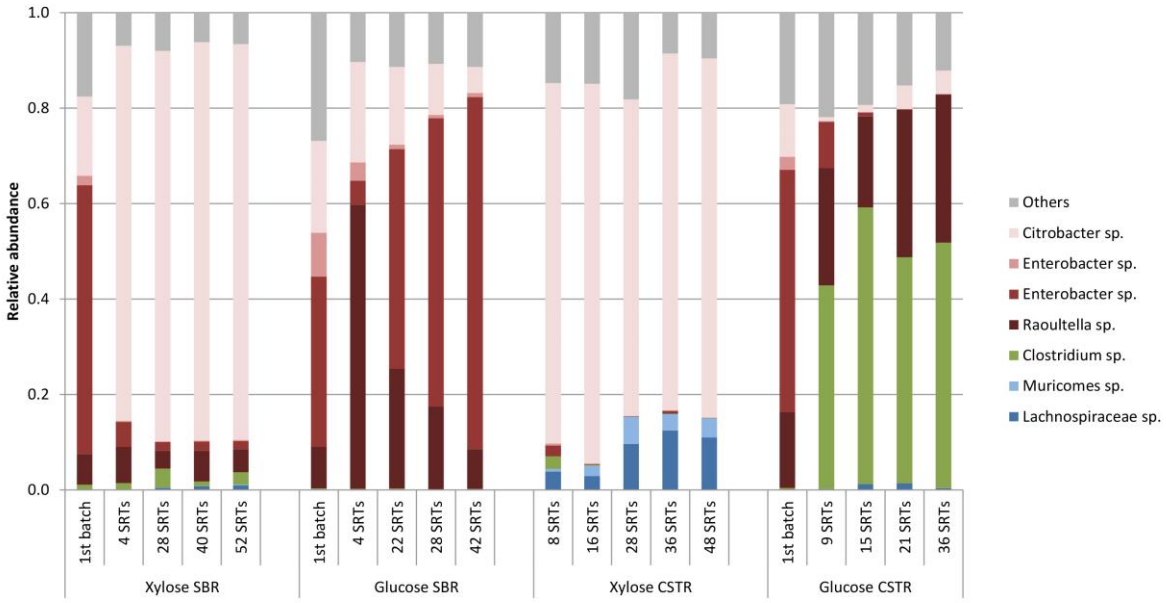

Figure 3: Overview of the amplicon results on the V3-V4 region of the 16S rRNA gene on OTU level. All OTUs that contribute to <1% of the reads are grouped into the others fraction (grey). In red OTUs belonging to the *Enterobacteriaceae* family are denoted, in green OTUs belonging to the *Clostridiaceae* family and in blue OTUs belonging to the *Lachnospiraceae* family. Closest related relatives found by BLAST used to characterize the OTU up to genus level (Appendix V). OTUs matched at <97% are presented as species from a family.

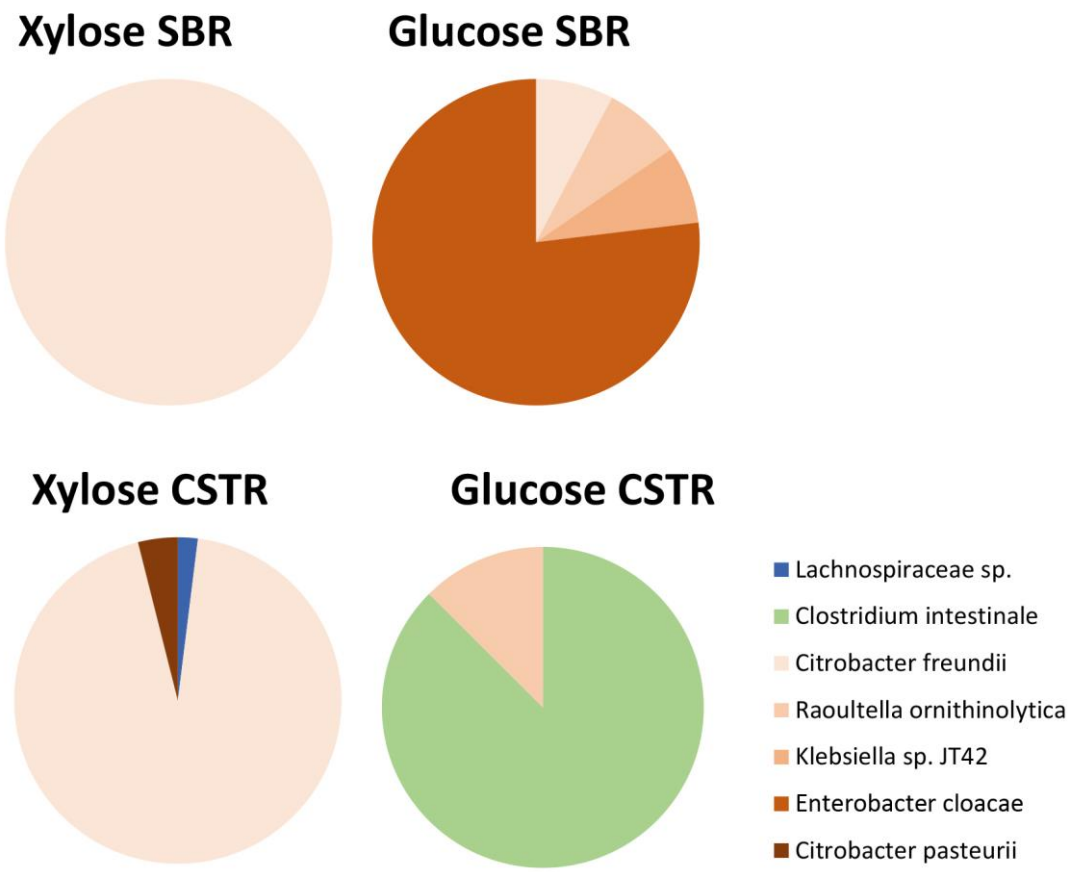

903

904

905 Figure 4: Result of the clone library analysis in which strains that were found as closest

906 relative (Appendix VII) are grouped into species

907

908